ADVANCED MATERIALS
www.advmat.de

Metal-Free Hydrogen-Bonded Polymers Mimic Noble Metal Electrocatalysts

*Halime Coskun, Abdalaziz Aljabour, Phil de Luna, He Sun, Nobuyuki Nishiumi, Tsukasa Yoshida, Georg Koller, Michael G. Ramsey, Theresia Greunz, David Stifter, Moritz Strobel, Sabine Hild, Achim Walter Hassel, Niyazi Serdar Sariciftci, Edward H. Sargent, and Philipp Stadler**

The most active and efficient catalysts for the electrochemical hydrogen evolution reaction (HER) rely on platinum, a fact that increases the cost of producing hydrogen and thereby limits the widespread adoption of this fuel. Here, a metal-free organic electrocatalyst that mimics the platinum surface by implementing a high work function and incorporating hydrogen-affine hydrogen bonds is introduced. These motifs, inspired from enzymology, are deployed here as selective reaction centres. It is shown that the keto-amine hydrogen-bond motif enhances the rate-determining step in proton reduction to molecular hydrogen. The keto-amine-functionalized polymers reported herein evolve hydrogen at an overpotential of 190 mV. They share certain key properties with platinum: a similar work function and excellent electrochemical stability and chemical robustness. These properties allow the demonstration of one week of continuous HER operation without notable degradation nor delamination from the carrier electrode. Scaled continuous-flow electrolysis is reported and 1 L net molecular hydrogen is produced within less than 9 h using 2.3 mg of polymer electrocatalyst.

Efficient hydrogen evolution reaction (HER) electrocatalysts require minimum binding energies for adsorbed (atomic) hydrogen ΔG_H^* along with a surface configuration that will reduce protons in an acidic environment as quantified via the thermodynamic exchange current i_0.[1–3] Only when these requirements are met will hydrogen evolution occur at minimum overpotential—a demanding level of performance needed for energetically efficient electrosynthesis of hydrogen from water. Further, for industrial operation, electrocatalysts must operate in aqueous media without degradation. Only a select few metals and metal compounds fulfill these requirements: platinum, rhodium, iridium, and their alloys; and compounds such as molybdenum and cobalt carbides, phosphides, sulfides, and phosphosulfides.[4–25] Mo-based systems (MoS_2,[10,26–30] MoP,[7] MoPS,[6] MoS_2–Cu_2S,[31] and MoC[18]) and carbon-nitride systems[32–34] represent the best-performing abundant alternatives to Pt (and Rh, Ir) for more cost-effective hydrogen production catalysts. Here, we instead explore conducting polydopamine (PDA) as electrocatalysts whose organic surfaces offer a remarkable degree of catalytic activity by tuning structural designs and conductivity.[35,36] We first sought to engineer a high work function, as this has

Dr. H. Coskun, Dr. A. Aljabour, Prof. N. S. Sariciftci
Institute of Physical Chemistry
Johannes Kepler University Linz
Altenberger Strasse 69, Linz 4040, Austria

Dr. P. de Luna, Prof. E. H. Sargent
Department of Materials Science and Engineering and the Edward S. Rogers Sr. Department of Electrical and Computer Engineering
University of Toronto
10 King's College Road, Toronto, Ontario M5S 3G4, Canada

Dr. H. Sun, N. Nishiumi, Prof. T. Yoshida
Research Center for Organic Electronics (ROEL)
Faculty of Engineering
Yamagata University
4-3-16 Jonan, Yonezawa, Yamagata 992-8510, Japan

Prof. M. G. Ramsey, Prof. G. Koller
Department of Physics
University of Graz
Universitätsplatz 5, Graz 8010, Austria

Dr. T. Greunz, Prof. D. Stifter
Center for Surface and Nanoanalytics (ZONA)
Johannes Kepler University Linz
Altenberger Strasse 69, Linz 4040, Austria

Dr. M. Strobel, Prof. S. Hild
Institute for Polymer Science
Johannes Kepler University Linz
Altenberger Strasse 69, Linz 4040, Austria

Prof. A. W. Hassel
Institute for Chemical Technology of Inorganic Materials
Johannes Kepler University Linz
Altenberger Strasse 69, Linz 4040, Austria

Dr. P. Stadler
Institute of Physical Chemistry and Linz Institute of Technology
Johannes Kepler University Linz
Altenberger Strasse 69, Linz 4040, Austria
E-mail: philipp.stadler@jku.at

The ORCID identification number(s) for the author(s) of this article can be found under https://doi.org/10.1002/adma.201902177.

DOI: 10.1002/adma.201902177

previously been reported to contribute to an optimized i_0.[3] In parallel, we needed to minimize the hydrogen binding energy ΔG_H^* to achieve surface adsorption energies similar to those of Pt. We found conducting biopolymers to be excellent candidates: they consist of (p-doped) positively charged insoluble polycations functionalized with electroactive hydrogen bonds.[35,36] They exhibit electrical conductivity greater than 0.1 S cm^{-1} sufficient to minimize parasitic electrode resistances and work functions ϕ deeper than –5.0 eV—ideal for HER. However, to increase ϕ further and, in parallel, to minimize the hydrogen affinity, we had to modify the hydrogen-bonded structure by embedding motifs that exhibit low ΔG_H^* into the polymers backbone. Using density functional theory, we identify keto-indoleamine hydrogen-bonds as favorable to drive the reaction. This catalytic site possesses a low ΔG_H^* at 220 meV, leading to favorable energetics to enhance the rate-determining Tafel recombination step. We predicted that it will produce molecular hydrogen at a high rate without requiring a metal site. We sought an experimental method to activate the keto-indoleamine motifs in the PDA structure. PDA gas phase synthesis at a high reaction temperature led to a high oxidation power and selective promotion of the keto-indoleamine motifs that significantly enhanced H_2 production and lowered the overpotential. We find that, upon keto-indoleamine activation, PDA exhibits surface characteristics similar to those of noble metals—low ΔG_H^* (similar to Ni) and ϕ (5.6 eV, similar to Ir). In addition it exhibited (electro)chemical robustness in aqueous acidic media. These features combine to provide a novel HER electrocatalyst that shows continuous hydrogen production at minimum losses and without notable degradation over an initial 300 h operation period.

Conductive biopolymers employ electroactive hydrogen-bonded functional motifs that are an integral part of the conjugated-conductive system.[35–37] We hypothesized that these bonds can be utilized for the HER, since the proton adsorption and recombination can occur similarly as on catalytic metals. We first analyzed the different types of hydrogen bonds in polydopamine (PDA)[38–48] using ab initio calculations and estimated the binding energy of each type of hydrogen bonds for the Volmer reaction (**Figure 1**). The four prototypes of hydrogen-bonds in PDA are a result of the intermediate oxidation products of dopamine formed during polymerization (Figure 1a):[37–39] On top of dopamine (DA) this includes dopaminequinone (DAQ), leucodopaminechrome (LDC) and, the ultimate oxidation intermediate, 5,6-dihydroxyindole (DHI). The amines of LDC and DHI are of secondary type (indole- or indoline-amine), while DA and DAQ have a primary amine. From that, four types of hydroxyl- and keto-amine hydrogen bonds are present in PDA: the hydroxyl-indoleamines (**1**, OH-HN_{DHI}); the keto-indoleamines (**2**, O-HN_{DHI}); the hydroxyl-dopamine (**3**, OH-$H_2N_{DA/DAQ}$); and ultimately the keto-indolineamine (**4**, O-HN_{LDC}). Previous polymerization reactions have shown that the primary amines (DA and DAQ) quantitatively outnumber the indole- and indoline- amines (LDC and DHI).[39]

In computational studies, we noticed that the basicity of the corresponding nitrogen group causes a significant change in the affinity toward HER: DA and DAQ are soluble in water (partly protonated, pK_a are 8.9 and 9.3, respectively), while LDC

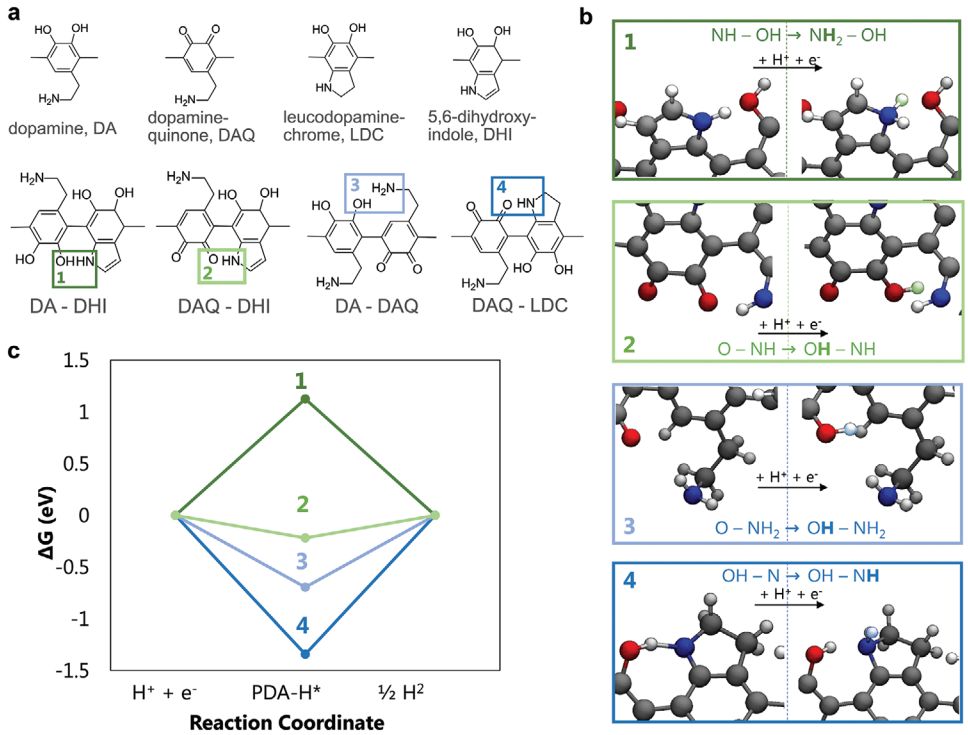

Figure 1. DFT calculation of the hydrogen affinity of hydrogen bonding. a) Monomer units in polydopamine (PDA) and illustration of the four dominant hydrogen-bonded motifs. b) Simulation of Volmer reaction on the hydroxyl-indoleamine (**1**, DA-DHI), keto-indoleamine (**2**, DAQ-DHI), the hydroxyl-dopamine (**3**, DA-DAQ) and the keto-indolineamine (**4**, DAQ-LDC). c) Reaction energy diagrams for HER on the distinct motifs. The keto-indoleamine group (**2**, DAQ-DHI) offers the lowest energy for ΔG_H^* (–0.22 eV) while the other hydrogen-bonded motifs possess unfavorable energies for HER.

and DHI are insoluble and slightly acidic (pK_a-values ≈ 6.5). The shift in pK_a is reflected in DFT simulations of the motifs in terms of its binding energy of adsorbed hydrogen H* (i.e., the Volmer reaction, Figure 1b,c): the optimum (lowest) energy (ΔG_H^* = –0.22 eV) was observed for the keto- indoleamine motifs (O-HN_{DHI}, marked as function **2**). DFT calculations reveal that Gibbs free energy of this reaction is significantly lower compared to that for the other motifs, especially those that involve primary (and basic) amines (i.e., DA and DAQ-based units) (Figure 1). We conclude that HER selectivity can be enhanced by promoting the number of keto-indoleamine functional groups in the PDA structure. This necessitates that the DHI building block must be implemented as the main repeating unit. To realize DHI-rich PDA (DHI-PDA) experimentally, we modified the polymerization step of the gas phase synthesis. We explored experimentally the reaction parameters of the previously reported oxidative chemical vapor deposition (oCVD schematic in Figure S15, Supporting Information).[37,39] DHI represents the uppermost oxidation byproduct in the dopamine oxidation cascade: we increased the amount of DHI prior to polymerization by amplifying the oxidation power, increasing the temperature in the reaction zone. We kept other parameters constant (oxidation reagent, pressure, gas flow), and increased temperature (i.e., ΔT = 50 °C from 300 to 350 °C) to form DHI-PDA without inducing overoxidation or compromising electrical conductivity (Figure S9, Supporting Information). For DHI-PDA, we confirmed the increased presence of DHI by scanning the Raman shift and by looking at the amines in the N1s response by XPS. In the first, the Raman modes in DHI-PDA show an explicit shoulder at 1587 cm^{-1}. This feature is strong in DHI monomer and comparatively lower in DHI-PDA and further reduced in PDA* (**Figure 2**b). Detailed fits of the Raman modes between the monomer DHI and DHI-PDA are discussed in Figures S11,S12 and Table S2, Supporting Information). Similar results were observed in XPS, where the sum of the DHI-amines (i.e., secondary amines and imines) make up 73% of the total N1s response, while standard synthesized PDA* has only 33% of DHI-amines (Figure 2c). Both results indicate that we synthesized a DHI-dominated polymer with 73% DHI-amines as the main building unit (DHI-PDA). In addition, the work function ϕ (Figure S7, Supporting Information, UV-photoemission) in DHI-PDA (5.6 eV) is comparatively higher than PDA* (5.25 eV), sitting between that of Ni (5.25 eV) and Ir (5.75 eV) (Figure 2d). This is explained by the higher doping level, also confirmed by the strong presence of imines in the structure. The photoemission (UV and X-ray) results as well as the Raman spectra confirm that higher reaction temperature in the oCVD synthesis forms DHI-PDA with

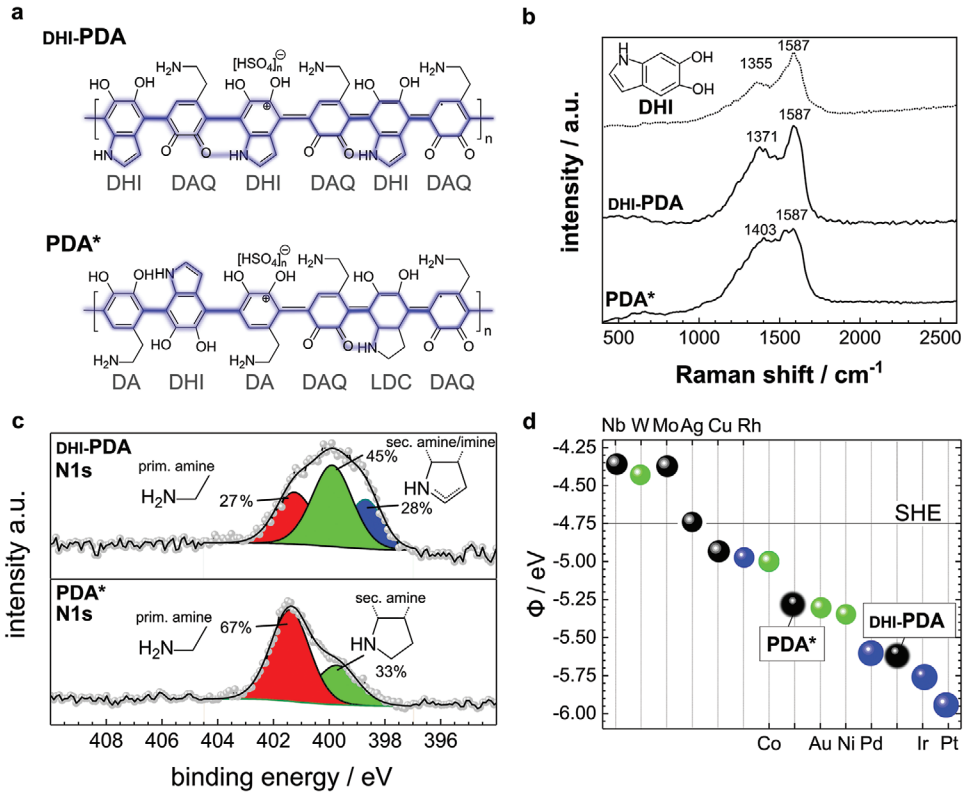

Figure 2. Electronic and structural properties of (DHI-)PDA. a) Statistical monomer of DHI-PDA and PDA* as-derived by X-ray photoelectron and Raman spectroscopy including the fragmental sequence (DA, dopamine; DAQ, dopaminequinone; LDC, leucodopaminechrome; DHI, dihydroxyindole). b) The Raman shifts show the explicit DHI-shoulder arising stronger in DHI-PDA than in the PDA* synthesized in less-oxidative surroundings. c) N1s photoelectron peaks of DHI-PDA compared to PDA*: The response shows the change in functionality, importantly on the nitrogen. While PDA has primary amines (R—NH_2 from DA and DAQ-themes) a major repeating unit, DHI-PDA has higher concentration of the oxidative derivative DHI unit seen by domination of secondary amine (R—NH—R) and imine (R=N—R) themes. d) Work functions of DHI-PDA and PDA* as compared various catalytic metals[56] and the standard hydrogen electrode (SHE). All photoemission experiments (UV and X-ray) were carried out directly on carbon felt.

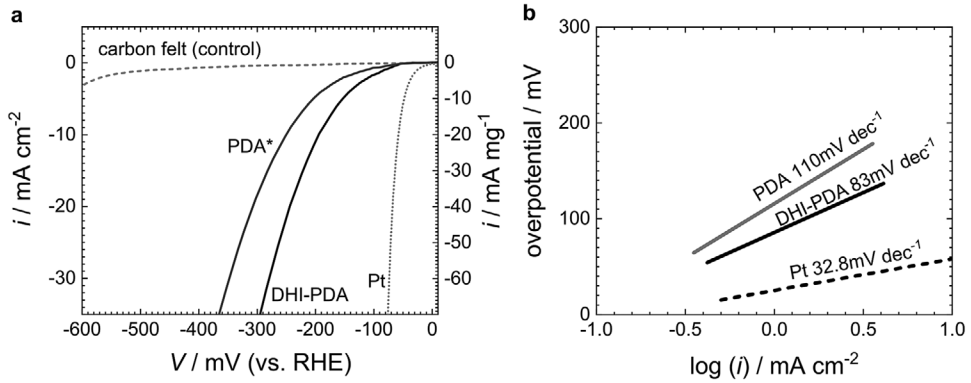

Figure 3. Electrochemical characterization. a) Voltammetric scans (10 mV s^{-1}, referred to active area and gravimetric) in 1 M TfOH electrolyte for HER showing the performance of PDA (standard) and DHI-PDA as compared to Pt (reference) and CF (blank control). b) Tafel plot (log (*i*) vs. η) with the slopes indicated in the graph. The reference overpotential η (at 10 mA cm^{-2} planar current density) is 190 mV (DHI-PDA) and 270 mV (PDA).

the (O-HN_{DHI}) motif as the major hydrogen bonding functional group as depicted in the statistical monomer (Figure 2a). As reported in earlier studies, PDAs generated through oCVD offers the advantage of direct deposition on large surface area electrodes such as carbon felt. oCVD can be used to produce optimized DHI-PDA HER electrodes possessing a large surface area allowing the study of electrochemical reaction in detail. The electrochemical studies (polarographic scans, chronoamperometry, and impedance) were performed using an H-cell (separated anode and cathode) with a separation membrane to minimize crossover. We used 1 M trifluoromethanesulfonic acid as the electrolyte (TfOH, activity of the protons is close to unity). We find the stability of this electrolyte system superior to sulfuric acid due to PDA's ability to reduce the sulfate anions of sulfuric acid. By introducing TfOH, we exclude side reactions and achieve a quantitative Faradaic yield (100% hydrogen). Cyclic voltammograms for DHI-PDA and standard PDA show electrocatalytic reduction currents for HER (**Figure 3**). For control samples we include a freshly etched Pt-standard electrode (dashed line) and blank carbon felt electrode (dots). For DHI-PDA we obtain the threshold current density (10 mA cm^{-2}) at –190 mV versus the reversible hydrogen electrode (RHE, activity of protons is unity, black line), while the standard PDA* (grey line) requires 120 mV higher potential (270 mV) to reach the same threshold current density. All scans are acquired at a 10 mV s^{-1} scan rate under stirring at ambient pressure and temperature (25 °C and 1 atm). The Tafel plots confirm the higher electroactivity of DHI-PDA at 80 mV dec^{-1} compared to 110 mV dec^{-1} for standard PDA*. In a separate experiment without stirring we use the voltammogram to estimate the exchange current densities i_0 for both PDA systems. For DHI-PDA the i_0 values are beyond catalytic Ni and below Ir (i.e., 1.2×10^{-5} A cm^{-2}), while i_0 for standard PDA* is an order of magnitude below (3.0×10^{-6} A cm^{-2}, details in Figure S9, Supporting Information). All current densities refer to the electrochemical active surface area A_{ECSA} measured by electrochemical impedance (Figures S7, S8, and S10, Supporting Information). Electrochemical characterization includes the relevant cell resistances from the electrolyte (3 Ω), the membrane (H-cell, 30 Ω) and the electrocatalyst ($\Delta R = 0.2$ Ω) as well as the capacitance of the (electrochemical) active area (C_i, DHI-PDA = 425 µF cm^{-2} or 10.625 cm^2 per projected area). To explore stability, we performed representative chronoamperometric transients with 300 h (12.5 days) continuous operation of HER at 10.9 mA cm^{-2} at –190 mV vs. RHE (**Figure 4**a–c). We observed continuous hydrogen (and oxygen) gas evolution as verified by gas chromatography with a ratio O_2:H_2 1:1.98 (Figure S17, Supporting Information). The ex situ SEM studies show that the catalyst remains on the surface (Figure 4c). The conductive polymer studied herein sustained performance in elelctrocatalytic HER. The DHI-PDA catalyst represents a homogeneously functionalized conductive polymer with rich keto-indoleamine hydrogen-bonded motifs acting as catalytic sites. Their role as active-site hydrogenation center is further studied using in situ IR, where the Volmer reaction emerges an addition hydrogen bond under cathodic bias (**Figure 5**a,b). Thus, the organic catalyst shares various electronic properties with catalytic metals. These properties include a similar mechanism, similar work function (comparable to Ir) and a similar proton adsorption energy ΔG_H^* (equal to Ni), leading to an exchange current density almost as high as these metals (i.e., DHI-PDA work function $\simeq$ 1 eV below the standard hydrogen potential, $\Delta G_H^* = 0.22$ eV, and i_0 at 1.2×10^{-2} mA cm^{-2} as shown in the volcano and Trasatti plot, Figure 5) 38. Further improvements in the electrocatalytic polymer can be achieved by increasing the surface density of catalytic sites, that is, the fraction of DHI-fragments to reach a similar exchange current density as noble metals such as Pt. The performance, insolubility in acidic electrolyte, and electrochemical stability allowed us to demonstrate a scaled electrolyser cell, in which we loaded various amounts of DHI-PDA to a carbon mesh area 3 cm^2. By increasing the catalyst load up to 2.3 mg, we can operate HER up to a current of 0.25 A (or 0.11 A mg^{-1} DHI-PDA) continuously. At this size we reach the geometric limit of the custom oCVD setup and thus we use the absolute current normalized to the total mass of catalyst loaded (i.e., mg polymer absolute on carbon felt) for comparison. We find that *i* scales nearly linearly with the mass load (mg DHI-PDA on the electrode). At 0.25 A (corresponding to a mass activity of 0.11 A mg^{-1}) we calculate a turnover frequency for HER at 0.2 s^{-1}. This number is obtained by using the total amount of DHI units inside DHI-PDA, that is, 73% net DHI of the total moles monomer units

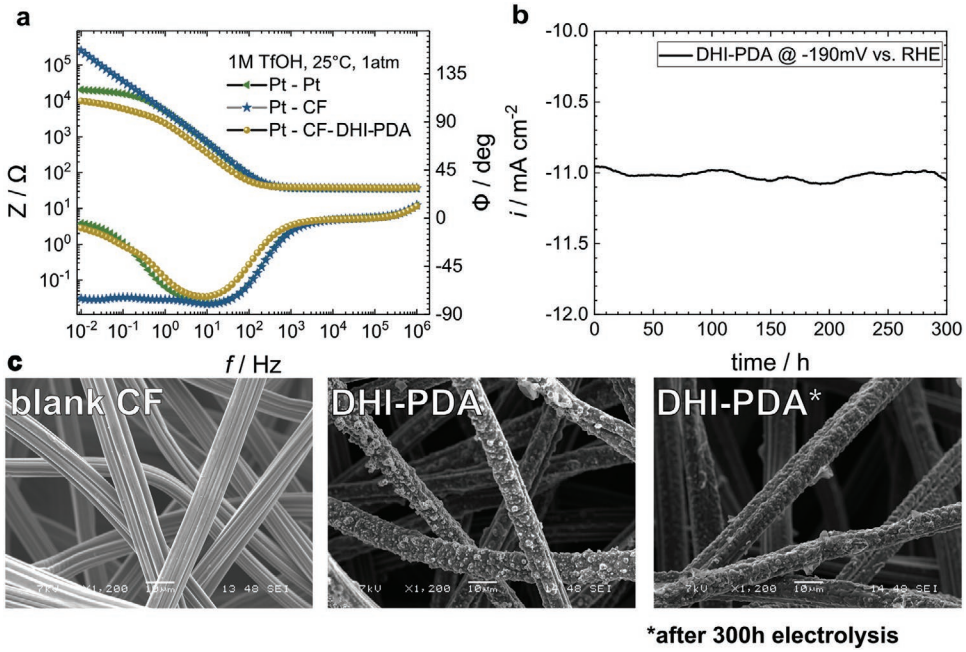

Figure 4. Impedance and chronoamperometric stability characterization. a) Bode-plot (frequency dependent electrochemical impedance) of 3-electrode setup showing the response of Pt-Pt (reference), Pt-CF (control) and Pt-CF+DHI-PDA working (and counter) electrodes. The resistance between control and DHI-PDA is marginally small (0.1 Ω). b) Chronoamperometric transients of DHI-PDA system over time without notable degradation (0.6% change at –190 mV vs. RHE). c) SEM scans on blank CF, DHI-PDA-coated CF before and after running a continuous electrolysis for 300 h.

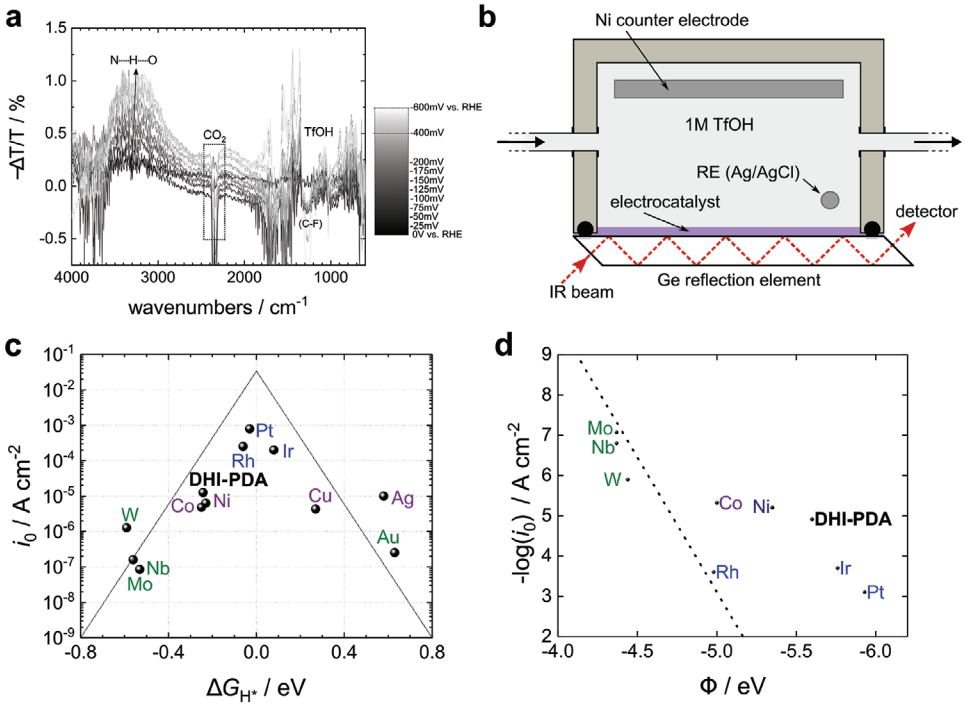

Figure 5. Mechanistic studies and Volcano and Trasatti plot.[3] a) In situ spectral IR showing the emergence of broad hydrogen-bonds at 3300 cm^{-1} under cathodic bias. b) Schematic of the flow-cell used for in situ IR (ATR-mode). c) The plot shows the exchange current density versus the hydrogen adsorption energy ΔG_H^* and the position of the DHI-PDA electrocatalyst as compared to metallic systems (i_0 between Ni and Ir at 1.2×10^{-5} A cm^{-2} at ΔG_H^* at –0.22 eV). d) The work function ϕ (here various catalytic metals) and log i_0 including Trasatti's empiric correlation (dashed line) pointing at potential improvements for DHI-PDA concerning i_0.

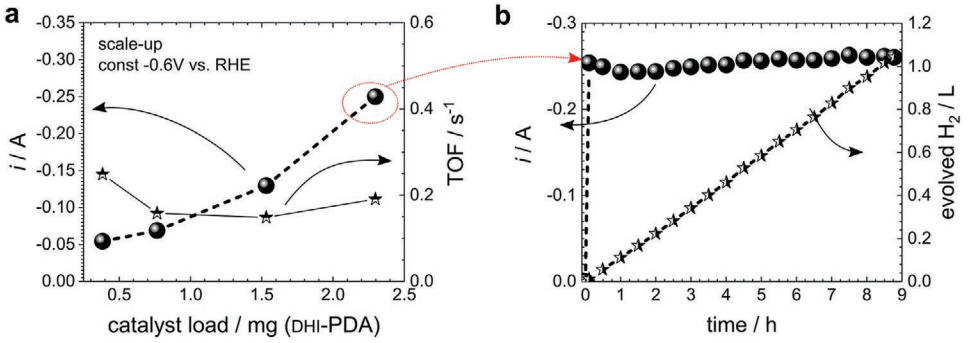

Figure 6. Demonstration of DHI-PDA electrolyzer. Carbon felt is used with different catalyst mass loadings and plotted versus absolute current *i* at −0.6 V vs. RHE. We include the turnover frequency (TOF) referred to the total amount of DHI monomer building blocks (73% according to the XPS N1s high resolution data). At 0.25 A (or mass activity of 0.11 A mg^{-1}) we show the continuous production of 1 L net hydrogen gas based on a flow cell with DHI-PDA carbon felt.

implemented in the system (the 73% DHI according to the XPS N1s high resolution data, Figure 2a). With that, we produce 1.0 L of hydrogen within 8.7 h of continuous electrolysis (**Figure 6**).

This work shows the ability to mimic a noble metal-like catalyst surface utilizing organic functional groups such as hydrogen-bonded motifs. These have attracted attention for catalytic applications, since various processes in enzymology utilize them for selective reaction processes. Here, we focus on the electrocatalytic proton reduction, that is, the affinity of such motifs to proceed as electrocatalyst. At the heart of this reaction is the two-step reduction process from protons to molecular hydrogen, that is, the Volmer and Tafel (or Heyrovsky) steps. The Tafel step (i.e., the recombination of adsorbed hydrogen H*) is rate-determining. Reducing the binding energy of the adsorbed hydrogen intermediate H* is therefore vital for the overall performance. We utilize, for the first time, a discrete functional motif (keto-indoleimines) as a catalytic reaction center that provides the optimal energetics for HER. Interestingly, these polymers possess a similar adsorption energy as metals (e.g., Ni), pointing to the power of bio-organic functional groups in electrocatalysis. This results in an efficient catalyst that exhibits quantitative Faradaic efficiency with a Tafel slope of 80 mV dec^{-1}, a low overpotential of 190 mV (at 10 mA cm^{-2}), and robust functionalized polyphenylene core[49] allowing long-term operation with no noticeable degradation for 300 h. The catalytic system, however, requires further optimization, in particular the up-concentration of the proton-active elements DHI in order to increase the planar active site density close to the noble metals. With that, we attempt to reach ultimately exchange currents close to noble metal systems. In terms of long-term stability in acidic electrolytes the present system is already competitive.

Experimental Section

Synthesis: Oxidative chemical vapor deposition (oCVD) was used to deposit the PDA and DHI-PDA directly on carbon felt (CF) (10 mm × 10 mm, SGL Group, The Carbon Company) (schematic of process Figure S16, Supporting Information). These electrodes were directly used for electrochemical studies. For the PDA-synthesis, dopamine hydrochloride (Sigma Aldrich) was dried for 10 h at 150 °C in inert atmosphere in the presence of CaH_2 (95%, Sigma Aldrich). For the polymerization reaction, oxidative chemical vapor deposition was employed. This consisted of a tube furnace (Carbolite company; glass tube length: 45 cm; tube diameter: 2.4 cm). In the reaction zone the temperature was set constant to 300 and 350 °C, respectively. Nitrogen (3 L min^{-1}) was used as carrier gas in a laminar flow. The entire process was carried out at atmospheric pressure (1 atm). In the reaction zone, sulfuric acid (95–97%, J.T. Baker) and sodium sulfate (≤99.0%, Sigma Aldrich) are prepared. Upon heating the acid was vaporized and immediately reacted with the gas-phase dopamine. By controlling the reaction time the desired film thickness of 0.5 mg per cm^2 carbon felt (30 min deposition time yields approximately 0.77 mg DHI-PDA on a 1 cm^2 carbon felt area) could be controlled. For conductivity measurements sapphire substrates (10 mm × 10 mm × 0.5 mm, CrysTec Kristalltechnologie) were used with Cr/Au (8 nm/100 nm) electrodes (van der Pauw geometry). All substrates were treated with acetone, isopropyl alcohol, Hellmanex-detergent (Hellma, 70 °C) and deionized water prior usage. Cr/Au contacts were deposited by PVD through a shadow mask.

Electrochemical Characterization: For the electrochemical measurements the electrodes were rinsed with the electrolyte (1 M TfOH) and then directly installed as working electrode. The as prepared DHI-PDA, PDA*, and blank carbon felt electrodes were electrochemically characterized for hydrogen evolution using an H-Cell configuration. Electrochemical and electrosynthesis experiments were performed using a JAISSLE Potentiostat Galvanostat IMP 88 PC. Carbon-felt (and the catalyst coated electrodes) were set as working electrodes, Ag/AgCl (3 M KCl, +210 mV vs. SHE) was set as reference electrode. 1 M trifluoromethanesulfonic acid (98%, Sigma-Aldrich) was used as electrolyte solution and nickel plate or glassy carbon as counter electrodes. The compartments of the H-cell were separated by a diaphragm. For the long-term chronoamperometry (300 h), the sealed compartments of the cell were purged with N_2 gas for at least 1 h and glassy carbon counter electrodes were used. All results were given relative to the RHE. An activity of unity was assumed in 1 M TfOH (RHE equal to SHE). Linear sweep voltammograms (10 mV s^{-1}) and chronoamperometric scans were conducted under stirring the electrolyte solution in the cathode system and under nitrogen inert gas. A sealed compartment was used to frequently conduct a quantitative H_2 yield, which was found to be close to 98–99% each using a TRACE Ultra Gas Chromatograph equipped with a thermal conductivity detector (TCD) for analyzing the amount of H_2 gas produced during electrolysis. No byproduct was found in this system. The anode space was continuously purged with nitrogen gas to suppress diffusion of the concomitantly formed oxygen to the cathode space (solubility of oxygen is 8.3 ppm at 25 °C and 1 atm.). The electrochemical setup was characterized by systematic impedance analysis using an IVIUM compactstat (The Netherlands). The open-circuit potential (OCP) was measured and based on that the electrochemical impedance spectra (biased at OCP) in the range from 1 MHz to 1 Hz (perturbation amplitude of 10 mV) in all relevant

electrode configurations (Pt-Pt, Pt-CF, Pt-CF-DHI-PDA, PT-CF-PDA*) were recorded. The electrochemically active surface area (A_{ECSA}) was determined by impedance at 40 ± 5 µF cm^{-2} for a flat reference-electrode (stainless steel) and 425 ± 25 µF cm^{-2} for PDA-covered CF yielding factor ≈10 higher electrode on flat carbon. For the gravimetric current density, a catalyst load of 0.52 mg per cm^2 CF was used. By oCVD the uppermost surface of CF covers with DHI-PDA (and PDA, respectively) was observed with hardly any infiltration. For determining i_0, a separate scan was used without stirring. All measurements referred to the A_{ECSA} (Figures S7,S8, and S10, Supporting Information). The scale-up demonstrator used carbon felt electrodes with different projected areas (0.5–3.0 cm^2). These were implemented as electrodes in a cell system. Chronoamperometric scans were conducted at constant 0.6 V vs. RHE potential and the current (and hydrogen evolved at a Faraday yield of practically unity) was referenced to the absolute mass of DHI-PDA electrocatalyst. From that the turnover frequency (TOF) was also calculated. The number of moles of monomer was therefore calculated using an average monomer mass (between DA, DAQ, LDC, and DHI, av. 149 g mol^{-1}) plus one fraction of sulfuric acid (98 g mol^{-1}). From the XPS N1s peak it was found that 73% of DHI-PDA actually was DHI-fragment (secondary amine and imines). This molar mass was referred to the total amount of electrons transferred on the electrode to derive the TOF. A consistent TOF number was found at 1 to 3 cm^2 at 0.19 s^{-1} each.

$$TOF = \frac{i_{abs}}{2F} \cdot \frac{1}{n_{active\ sites}} \tag{1}$$

and

$$n_{active\ sites} = \frac{m}{M_{DHI\text{-}PDA}} \cdot x_{DHI} \tag{2}$$

The TOF formula included the absolute mass m catalyst load on carbon felt divided by the molar mass of the average monomer unit $M_{DHI\text{-}PDA}$ and multiplied by the fraction of active sites (x_{DHI} in DHI-PDA) equal to 73% (Figure 2a), the Faraday constant F and the number of transferred electrons (2). Structural and spectroscopic characterization: The X-ray photoelectron experiments (XPS) as well as the ultraviolet photoemission experiments (UPS) were all carried out directly on carbon felt covered with DHI-PDA or PDA (as well as reference measurements of carbon felt). UPS allowed to extract the work functions (spectrum shown in Supporting Information), while from XPS measurements chemical information from the C1s, the N1s, the O1s, and the S2p high resolution spectra were obtained. The latter practically only showed sulfur as part from the sulfate anion inside PDA and DHI-PDA. From the N1s peak the fraction of primary amine (C—NH$_2$), secondary amine (C—NH—C and ternary amine (C=N—C) was determined. The elemental high resolution scans (O1s, C1s and S2p and surveys including UPS) are presented in Figures S1– S6, Supporting Information. The XPS analysis was performed on a commercial ThermoFisher Theta Probe system equipped with an AlK$_\alpha$ (1486.7 eV) source. Charge compensation was achieved by a Dual Flood Gun system (1–2 eV electrons and Ar$^+$ ions), and the lens mode was set to standard. The energy pass amounted to 200 eV for the survey scan and to 50 eV for high-resolution (HR) scans, with energy steps of 1 and 0.1 eV, respectively. The Avantage v5.32 software package was employed for data analysis. The data fittings were in agreement with results described in the literature. The elemental concentrations and work functions were determined by survey- and high-resolution scans. Raman data were gathered using a WITec Alpha 300 RA Raman-microscope (WITec GmbH, Ulm, Germany). The spectra were recorded at room temperature. A Nd:YAG-laser, with a wavelength of 532 nm and a laser intensity of 1 mW, was used for excitation. A grating with 600 g mm^{-1} was installed, supporting a spectral resolution below 4 cm^{-1}. For the measurements a Nikon Plan 100x objective lens (Nikon Corporation, Tokyo, Japan) was used. The integration times were selected at 3 s (20 accumulations).

DFT-Calculations: The Vienna Ab initio Simulation Package (VASP) was used to simulate all density functional theory (DFT) calculations.[50] The Perdew–Burke–Ernzerhof (PBE) generalized gradient approximation exchange correlation functional was used with the all-electron frozen-core projector augmented wave (PAW) method.[51,52] Blöchl plane wave basis sets with a cutoff energy of 500 eV and a Fermi smearing width of 0.1 eV were used.[53] Long-range van der Waals interactions and dipole corrections were used. Monkhorst–Pack mesh was used for k-point sampling with 3 × 2 × 1 k-points sampled for the structure optimization.[53] Structural and unit cell optimizations were performed until the maximum cutoff was less than 0.02 eV per atom with the structures being fully optimized. The four monomer repeating unit was placed in a periodic box of size 17 Å × 24 Å × 15 Å with at least 10 Å of vacuum space placed between periodic images. Protons were initially placed between the amino and carbonyl groups in the hydrogen bond motif of each monomer as a starting point and then fully relaxed. The Atomic Simulation Environment (ASE)[54] was used to calculate thermodynamic quantities. The Gibbs free energies were calculated at 298 K and 1 atm as outlined below:

$$G = H - T \cdot S = E_{DFT} + E_{ZPE} + \int_0^{298K} C_v \cdot dT - T \cdot S \tag{3}$$

where E_{DFT} is the DFT calculated electronic energy, E_{ZPE} is the zero-point vibrational energy, $\int_0^{298K} C_v \cdot dT$ is the heat capacity, T is the temperature, and S is the entropy. Gas phase molecule H_2 was treated using the ideal gas approximation while adsorbate H* was treated using a harmonic approximation. The computational hydrogen electrode model (CHE)[55] was used to calculate the change in Gibbs free energy, ΔG, between reaction steps HER as outlined below:

$$H^+ + e^- + * \rightarrow H^* \tag{4}$$

$$H^* + H^+ + e^- \rightarrow H_2 \tag{5}$$

where * represents either a vacant surface catalytic active site, or intermediate species adsorbed on the active site. All data needed to evaluate the conclusions in the paper are present in the paper and/or the Supporting Information. Additional data are available from authors upon request.

Supporting Information

Supporting Information is available from the Wiley Online Library or from the author.

Acknowledgements

P.S., A.A., H.S., N.N., and T.Y. acknowledge the Austrian Science Fund (FWF) for the international joint project FWF I3822-N37 (Sustainable Catalysis). P.S. acknowledges the Government of Upper Austria within the Sabbatical program "Internationalization of the University of Linz". P.S. acknowledges the Linz Institute of Technology (LIT) and the Upper Austrian Government for the project Biopolymer Carbonate Reduction (CarboRed, LIT-2017-4-YOU-005). A.A. and A.W.H. gratefully acknowledge financial support from the Austrian Federal Ministry of Science, Research and Economy and the National Foundation for Research, Technology and Development in the frame of the Christian Doppler Laboratory COMBOX. P.D.L acknowledges the Natural Sciences and Engineering Research Council (NSERC) of Canada for financial support in the form of a Canadian Graduate Scholarship – Doctoral (CGS-D) award.

Conflict of Interest

The authors declare no conflict of interest.

Keywords

conducting polymers, electrocatalysis, hydrogen bonds, hydrogen evolution reaction, polydopamine

Received: April 5, 2019
Revised: April 15, 2020
Published online: May 17, 2020

[1] A. Zuttel, A. Remhof, A. Borgschulte, O. Friedrichs, *Philos. Trans. R. Soc., A* **2010**, *368*, 3329.
[2] Z. W. Seh, J. Kibsgaard, C. F. Dickens, I. Chorkendorff, J. K. Nørskov, T. F. Jaramillo, *Science* **2017**, *355*, eaad4998.
[3] S. Trasatti, *J. Electroanal. Chem. Interfacial Electrochem.* **1972**, *39*, 163.
[4] J. Miao, F.-X. Xiao, H. B. Yang, S. Y. Khoo, J. Chen, Z. Fan, Y.-Y. Hsu, H. M. Chen, H. Zhang, B. Liu, *Sci. Adv.* **2015**, *1*, e1500259.
[5] F. Li, X. Zhao, J. Mahmood, M. S. Okyay, S.-M. Jung, I. Ahmad, S.-J. Kim, G.-F. Han, N. Park, J.-B. Baek, *ACS Nano* **2017**, *11*, 7527.
[6] J. Kibsgaard, T. F. Jaramillo, *Angew. Chem., Int. Ed.* **2014**, *53*, 14433.
[7] P. Xiao, M. A. Sk, L. Thia, X. Ge, R. J. Lim, J.-Y. Wang, K. H. Lim, X. Wang, *Energy Environ. Sci.* **2014**, *7*, 2624.
[8] E. J. Popczun, C. G. Read, C. W. Roske, N. S. Lewis, R. E. Schaak, *Angew. Chem.* **2014**, *126*, 5531.
[9] J. Xie, H. Zhang, S. Li, R. Wang, X. Sun, M. Zhou, J. Zhou, X. W. D. Lou, Y. Xie, *Adv. Mater.* **2013**, *25*, 5807.
[10] D. Voiry, M. Salehi, R. Silva, T. Fujita, M. Chen, T. Asefa, V. B. Shenoy, G. Eda, M. Chhowalla, *Nano Lett.* **2013**, *13*, 6222.
[11] M. D. Scanlon, X. Bian, H. Vrubel, V. Amstutz, K. Schenk, X. Hu, B. Liu, H. H. Girault, *Phys. Chem. Chem. Phys.* **2013**, *15*, 2847.
[12] D. Voiry, H. Yamaguchi, J. Li, R. Silva, D. C. B. Alves, T. Fujita, M. Chen, T. Asefa, V. B. Shenoy, G. Eda, M. Chhowalla, *Nat. Mater.* **2013**, *12*, 850.
[13] H. Zhang, P. An, W. Zhou, B. Y. Guan, P. Zhang, J. Dong, X. W. D. Lou, *Sci. Adv.* **2018**, *4*, eaao6657.
[14] Y. B. Mollamahale, N. Jafari, D. Hosseini, *Mater. Lett.* **2018**, *213*, 15.
[15] R. Bose, V. R. Jothi, B. Koh, C. Jung, S. C. Yi, *Small* **2018**, *14*, 1703862.
[16] Z. Zhuang, Y. Li, Z. Li, F. Lv, Z. Lang, K. Zhao, L. Zhou, L. Moskaleva, S. Guo, L. Mai, *Angew. Chem., Int. Ed.* **2018**, *57*, 496.
[17] C. Tan, Z. Luo, A. Chaturvedi, Y. Cai, Y. Du, Y. Gong, Y. Huang, Z. Lai, X. Zhang, L. Zheng, X. Qi, M. H. Goh, J. Wang, S. Han, X.-J. Wu, L. Gu, C. Kloc, H. Zhang, *Adv. Mater.* **2018**, *30*, 1705509.
[18] S. Jing, L. Zhang, L. Luo, J. Lu, S. Yin, P. K. Shen, P. Tsiakaras, *Appl. Catal., B* **2018**, *224*, 533.
[19] J. Li, P. Liu, Y. Qu, T. Liao, B. Xiang, *Int. J. Hydrogen Energy* **2018**, *43*, 2601.
[20] V. Fominski, R. Romanov, D. Fominski, P. Dzhumaev, I. Troyan, *Opt. Laser Technol.* **2018**, *102*, 74.
[21] E. Demir, S. Akbayrak, A. M. Önal, S. Özkar, *ACS Appl. Mater. Interfaces* **2018**, *10*, 6299.
[22] D. Voiry, H. S. Shin, K. P. Loh, M. Chhowalla, *Nat. Rev. Chem.* **2018**, *2*, 0105.
[23] J. Hu, B. Huang, C. Zhang, Z. Wang, Y. An, D. Zhou, H. Lin, M. K. H. Leung, S. Yang, *Energy Environ. Sci.* **2017**, *10*, 593.
[24] J. Hu, C. Zhang, X. Meng, H. Lin, C. Hu, X. Long, S. Yang, *J. Mater. Chem. A.* **2017**, *5*, 5995.
[25] T. Liu, D. Liu, F. Qu, D. Wang, L. Zhang, R. Ge, S. Hao, Y. Ma, G. Du, A. M. Asiri, L. Chen, X. Sun, *Adv. Energy Mater.* **2017**, *7*, 1700020.
[26] T. F. Jaramillo, K. P. Jorgensen, J. Bonde, J. H. Nielsen, S. Horch, I. Chorkendorff, *Science* **2007**, *317*, 100.
[27] H. Li, C. Tsai, A. L. Koh, L. Cai, A. W. Contryman, A. H. Fragapane, J. Zhao, H. S. Han, H. C. Manoharan, F. Abild-Pedersen, J. K. Nørskov, X. Zheng, *Nat. Mater.* **2016**, *15*, 48.
[28] A. B. Laursen, S. Kegnæs, S. Dahl, I. Chorkendorff, *Energy Environ. Sci.* **2012**, *5*, 5577.
[29] J. D. Benck, Z. Chen, L. Y. Kuritzky, A. J. Forman, T. F. Jaramillo, *ACS Catal.* **2012**, *2*, 1916.
[30] J. Bonde, P. G. Moses, T. F. Jaramillo, J. K. Nørskov, I. Chorkendorff, *Faraday Discuss.* **2008**, *140*, 219.
[31] C. Bae, T. A. Ho, H. Kim, S. Lee, S. Lim, M. Kim, H. Yoo, J. M. Montero-Moreno, J. H. Park, H. Shin, *Sci. Adv.* **2017**, *3*, e1602215.
[32] J. Duan, S. Chen, M. Jaroniec, S. Z. Qiao, *ACS Nano* **2015**, *9*, 931.
[33] Y. Zheng, Y. Jiao, Y. Zhu, L. H. Li, Y. Han, Y. Chen, A. Du, M. Jaroniec, S. Z. Qiao, *Nat. Commun.* **2014**, *5*, 3783.
[34] X. Liu, L. Dai, *Nat. Rev. Mater.* **2016**, *1*, 16082.
[35] H. Coskun, A. Aljabour, W. Schöfberger, A. Hinterreiter, D. Stifter, N. S. Sariciftci, P. Stadler, *Adv. Mater. Interfaces* **2019**, 1901364.
[36] H. Coskun, A. Aljabour, P. De Luna, D. Farka, T. Greunz, D. Stifter, M. Kus, X. Zheng, M. Liu, A. W. Hassel, W. Schöfberger, E. H. Sargent, N. S. Sariciftci, P. Stadler, *Sci. Adv.* **2017**, *3*, e1700686.
[37] H. Coskun, A. Aljabour, L. Uiberlacker, M. Strobel, S. Hild, C. Cobet, D. Farka, P. Stadler, N. S. Sariciftci, *Thin Solid Films* **2018**, *645*, 320.
[38] R. A. Zangmeister, T. A. Morris, M. J. Tarlov, *Langmuir* **2013**, *29*, 8619.
[39] J. Liebscher, R. Mrówczyński, H. A. Scheidt, C. Filip, N. D. Hădade, R. Turcu, A. Bende, S. Beck, *Langmuir* **2013**, *29*, 10539.
[40] A. Napolitano, V. Ball, C.-t. Chen, M. J. Buehler, *Acc. Chem. Res.* **2014**, *47*, c3541.
[41] V. Ball, D. D. Frari, V. Toniazzo, D. Ruch, *J. Colloid Interface Sci.* **2012**, *386*, 366.
[42] X. Jiang, Y. Wang, M. Li, *Sci. Rep.* **2015**, *4*, 6070.
[43] V. Ball, D. Del Frari, M. Michel, M. J. Buehler, V. Toniazzo, M. K. Singh, J. Gracio, D. Ruch, *BioNanoScience* **2012**, *2*, 16.
[44] Y. Liu, K. Ai, L. Lu, *Chem. Rev.* **2014**, *114*, 5057.
[45] M. E. Lynge, R. van der Westen, A. Postma, B. Städler, *Nanoscale* **2011**, *3*, 4916.
[46] M. Sheliakina, A. B. Mostert, P. Meredith, *Mater. Horiz.* **2018**, *5*, 256.
[47] D. J. Carrad, A. B. Mostert, A. R. Ullah, A. M. Burke, H. J. Joyce, H. H. Tan, C. Jagadish, P. Krogstrup, J. Nygård, P. Meredith, A. P. Micolich, *Nano Lett.* **2017**, *17*, 827.
[48] M. D'Ischia, K. Wakamatsu, F. Cicoira, E. Di Mauro, J. C. Garcia-Borron, S. Commo, I. Galván, G. Ghanem, K. Kenzo, P. Meredith, A. Pezzella, C. Santato, T. Sarna, J. D. Simon, L. Zecca, F. A. Zucca, A. Napolitano, S. Ito, *Pigm. Cell Melanoma Res.* **2015**, *28*, 520.
[49] M. Adamski, T. J. G. Skalski, B. Britton, T. J. Peckham, L. Metzler, S. Holdcroft, *Angew. Chem.* **2017**, *129*, 9186.
[50] M. Matsumoto, T. Miyazaki, H. Imai, *J. Phys. Chem. C* **2011**, *115*, 11163.
[51] J. P. Perdew, K. Burke, M. Ernzerhof, *Phys. Rev. Lett.* **1996**, *77*, 3865.
[52] P. E. Blöchl, *Phys. Rev. B* **1994**, *50*, 17953.
[53] G. Kresse, D. Joubert, *Phys. Rev. B* **1999**, *59*, 1758.
[54] A. Hjorth Larsen, J. Jørgen Mortensen, J. Blomqvist, I. E. Castelli, R. Christensen, M. Dułak, J. Friis, M. N. Groves, B. Hammer, C. Hargus, E. D. Hermes, P. C. Jennings, P. Bjerre Jensen, J. Kermode, J. R. Kitchin, E. Leonhard Kolsbjerg, J. Kubal, K. Kaasbjerg, S. Lysgaard, J. Bergmann Maronsson, T. Maxson, T. Olsen, L. Pastewka, A. Peterson, C. Rostgaard, J. Schiøtz, O. Schütt, M. Strange, K. S. Thygesen, T. Vegge, L. Vilhelmsen, M. Walter, Z. Zeng, K. W. Jacobsen, *J. Phys.: Condens. Matter* **2017**, *29*, 273002.
[55] A. A. Peterson, F. Abild-Pedersen, F. Studt, J. Rossmeisl, J. K. Nørskov, *Energy Environ. Sci.* **2010**, *3*, 1311.
[56] *Electronic and Vibrational Properties* (Ed: G. Chiarotti), volume 24b of *Landolt-Börnstein - Group III Condensed Matter*, Springer-Verlag, Berlin/Heidelberg, Germany **1994**.